

An exact finite strip for the calculation of relative post-buckling stiffness of isotropic plates

H. R. Ovesy[†]

*Aerospace Engineering Department and Centre of Excellence in Computational Aerospace Engineering,
Amirkabir University of Technology, Tehran, Iran*

S. A. M. Ghannadpour[‡]

*Space Engineering Department, Faculty of New Technologies and Energy Engineering,
Shahid Beheshti University, G.C., Evin, 1983963113, Tehran, Iran*

(Received December 17, 2007, Accepted December 30, 2008)

Abstract. This paper presents the theoretical developments of an exact finite strip for the buckling and initial post-buckling analyses of isotropic flat plates. The so-called exact finite strip is assumed to be simply supported out-of-plane at the loaded ends. The strip is developed based on the concept that it is effectively a plate. The present method, which is designated by the name Full-analytical Finite Strip Method in this paper, provides an efficient and extremely accurate buckling solution. In the development process, the Von-Karman's equilibrium equation is solved exactly to obtain the buckling loads and the corresponding form of out-of-plane buckling deflection modes. The investigation of thin flat plate buckling behavior is then extended to an initial post-buckling study with the assumption that the deflected form immediately after the buckling is the same as that obtained for the buckling. It is noted that in the present method, only one of the calculated out-of-plane buckling deflection modes, corresponding to the lowest buckling load, i.e., the first mode is used for the initial post-buckling study. Thus, the post-buckling study is effectively a single-term analysis, which is attempted by utilizing the so-called semi-energy method. In this method, the Von-Karman's compatibility equation governing the behavior of isotropic flat plates is used together with a consideration of the total strain energy of the plate. Through the solution of the compatibility equation, the in-plane displacement functions which are themselves related to the Airy stress function are developed in terms of the unknown coefficient in the assumed out-of-plane deflection function. These in-plane and out-of-plane deflected functions are then substituted in the total strain energy expressions and the theorem of minimum total potential energy is applied to solve for the unknown coefficient. The developed method is subsequently applied to analyze the initial post-buckling behavior of some representative thin flat plates for which the results are also obtained through the application of a semi-analytical finite strip method. Through the comparison of the results and the appropriate discussion, the knowledge of the level of capability of the developed method is significantly promoted.

Keywords: exact strip; relative stiffness; initial post-buckling stage; von-kármán's compatibility and equilibrium equations.

[†] Associate Professor, Ph.D., E-mail: Ovesy@aut.ac.ir

[‡] Ph.D., E-mail: Ghannadpour@aut.ac.ir

1. Introduction

Prismatic plates and plate structures are increasingly used as structural components in various branches of engineering, chief of which are aerospace and marine engineering. These structures are often employed in situations where they are subjected to in-plane compressive loading. In aerospace, in particular, the quest for efficient, light-weight structures often leads to allowing for the possibility of local buckling and post-local-buckling at design load levels. Thus it is important to accurately predict the buckling and post buckling behavior of such structures.

In the field of linear buckling and vibration analysis of composite laminated plates and plate structures formed of composite materials having very general material properties, Lau and Hancock 1984, Dawe and Craig 1988, Wang and Dawe 1999, Zou and Lam 2002 and Cheung and Kong 1995 have extensively used the finite strip method based on the use of both Classical Plate Theory (CPT), first-order Shear Deformation Plate Theory (SDPT) and Higher-order Shear Deformation Plate Theory (HSDPT).

The post-local-buckling behavior of elastic plates or plate structures is a geometric non-linear problem. The non-linearity occurs as a result of relatively large out-of-plane deflections, which necessitates the inclusion of non-linear terms in the strain-displacement equations. Inside the post-buckling region, the out-of-plane deflections grow in a stable manner as the load increases (i.e., as the load increases beyond its critical local buckling value). The growth in the out-of-plane deflections is accompanied by continuous alterations in the stress system within the cross section. The changes in out-of-plane deflections and the alteration in the stress system cause the compressional stiffness of the plate to decrease.

The non-linear equations governing the elastic large deflection of flat plates were first derived by von Kármán. The post-local-buckling behavior of a plate can be analyzed by solving the von Kármán non-linear equations, together with the appropriate boundary conditions. Unfortunately, the von Kármán equations are coupled and fourth order, and thus no rigorous solutions are available. This clearly indicates that the extension of the non-linear equations from a single plate analysis to the plate structure analysis will involve even more complexity. All these have prepared the ground for the development of the approximate methods to solve the post-local-buckling problem of plates and plate structures. These approximate methods are primarily based on the Principle of Minimum Potential Energy.

Among the energy-based approximate methods, the finite element method (FEM) has become the dominant form of geometrically non-linear structural analysis. However, although the finite element method has no limitation regarding boundary conditions and local discontinuities such as openings in plates, the large number of degrees of freedom, and thus considerable computational effort required in the non-linear analysis of plates and plate structures may be considered as a deterrent factor.

For the case of prismatic structures, the finite strip method (FSM) Graves Smith and Sridharan 1978 & 1981, which is a special form of the finite element method, has proved to be a capable tool for analyzing the post-buckling behavior of plates and plate structures. As far as the computational expense is concerned, the finite strip method can be significantly more efficient than the finite element method.

Early works concerned with the use of the FSM in predicting the geometrically non-linear response of single rectangular plates and prismatic plate structures are those of Graves Smith and Sridharan 1978 & 1981 and Hancock 1981. These authors consider the post-buckling behavior of plates with simply supported ends when subjected to progressive end shortening. They also consider

the post-buckling behavior of plate structures subjected to uniform or linearly varying end shortening with each component plate of the structure having simply supported ends. The elastic post-buckling response of channel section struts and rectangular box columns are investigated by Graves Smith and Sridharan. Hancock uses the finite strip method to investigate the post-buckling behavior of square box and I-section columns. In the finite strip methods developed by the aforementioned authors, in-plane displacement fields are postulated in addition to the out-of-plane displacement field. The lengthwise variations in the displacement fields are trigonometric functions. The crosswise variations in both in-plane and out-of-plane displacement fields are simple polynomial functions. It is noted that the above-mentioned finite strip methods can be categorized as Semi-analytical FSM (S-a FSM).

In another contribution, Dawe and Wang 1996 have developed a spline finite strip method for analyzing the geometrically non-linear response of rectangular composite laminated plates of arbitrary lay-up to progressive end shortening in their plane. The plates are assumed to be thin, thus allowing the analysis to be based on the use of classical plate theory. The attention is concentrated on a particular finite strip model whose displacement field uses cubic B-splines longitudinally, quadratic crosswise interpolation of the in-plane displacements and cubic crosswise interpolation of the out-of-plane displacement.

Kwon and Hancock 1992 have also developed a non-linear elastic Spline FSM to study the post-buckling behavior of isotropic thin-walled sections undergoing local and distortional buckling. The developed spline FSM takes account of geometric imperfections, residual stresses and non-simple boundary conditions at the ends of the section under study. The FSM is applied to predict the post-buckling behavior of lipped channel sections made of steel material. The comparison between the FSM results and the experimental results, obtained by the same authors in an earlier study, is found to be reasonable.

Kong and Cheung 1995 have developed a generalized geometrically non-linear spline finite strip for the analysis of plates. The finite strip is general in the sense that its formulation is based upon a third-order plate theory, and is applicable to thin plates as well as thick plates. The plates may be made of isotropic or laminated composite materials with small initial imperfections. The FSM is applied to analyze the post-buckling behavior of two isotropic square plates with small initial curvatures loaded in edge compression. For the readers' information, it is noted that Dawe 2002 provides a good state-of-the-art summary of the use of the finite strip methods in composite plates for both semi-analytical finite strip method (S-a FSM) and spline finite strip method.

Khong and Rhodes 1988 have set up a computationally efficient approach to the post-buckling analysis of prismatic structural members. In this approach, a linear finite strip method, developed for the buckling analysis, based on the Principle of Minimum Potential Energy is employed to find the buckling eigenvector. This eigenvector is then used as the post-buckled deflected shape in a single-term post-buckling analysis based on the Principle of Minimum Potential Energy. The analysis is simplified by the assumption that stresses in the direction perpendicular to loading and shear stresses have negligible effects. This approach can be considered as a lower bound method of post-buckling analysis (i.e., the post-buckling stiffness of the structure is underestimated by this approach). The method is applied to plain and stiffened channel sections as well as Z-sections.

An energy-based approximate method, referred to as the semi-energy method by Rhodes & Harvey 1977, was first used by Marguerre 1937, and has since been used by various researchers. It is worth mentioning that there are two papers, written by Rhodes 1996 and Chou & Rhodes 1997, which are extremely useful in providing references on the theoretical (mostly based on the semi-

energy method) and experimental research into thin-walled structures.

More recently, Ovesy *et al.* have developed a semi-energy post-local-buckling FSM in which the out-of-plane displacement of the finite strip is the only displacement which is postulated by a deflected form as distinct to that mentioned previously with respect to the S-a FSM and Spline FSM. The developed semi-energy FSM has been applied to analyze the post-local-buckling behavior of thin flat plates 2005, open channel section 2006 and box section struts 2006.

In this paper theoretical developments of an exact finite strip for the buckling and initial post-buckling analyses of isotropic flat plates are presented. The so-called exact finite strip is assumed to be simply supported out-of-plane at the loaded ends. The strip is developed based on the concept that it is effectively a plate, and thus the Von-Karman's equilibrium equation is solved exactly to obtain the general form of out-of-plane buckling deflection mode for the corresponding plate/strip and the Von-Karman's compatibility equation is subsequently solved exactly to obtain the general form of in-plane displacement fields in post-buckling region. This method is characterized by the use of buckling mode shapes, obtained from the Von-Karman's equilibrium equation, as global shape functions for representing displacements in a geometrically non-linear analysis. For this reason, this method is designated by the name Full-analytical Finite Strip Method (F-a FSM). In the cases of buckling and post-buckling analysis of plate, it can be modeled by assigning any arbitrarily given number of the developed exact finite strips across its width but very often one strip is adequately sufficient to model a plate.

2. Theoretical developments of the full-analytical FSM

In this section, the fundamental elements of the theory for the developed exact finite strip in buckling and post-buckling problems are outlined. It is noted that a perfectly flat exact strip made up of a linear isotropic material (with a constant modulus of elasticity E and Poisson ratio ν) is assumed throughout the theoretical developments of this paper. The so-called exact finite strip is assumed to be simply supported out-of-plane at the loaded ends, and be thin so that the Classical Plate Theory (CPT) is applied in the remaining of the paper.

2.1 Basic formulation of the problem

The exact finite strip, which is schematically shown in Fig. 1, is of length L , width b and thickness t . As mentioned earlier, the finite strip is simply supported out-of-plane at both ends, i.e., at ends $x = 0$ & L the boundary conditions are

$$w = w_{,y} = M_x = 0 \quad (1)$$

where the comma denotes partial differentiation, i.e., $(\)_{,x} = \partial(\)/\partial x$ and $(\)_{,xx} = \partial^2(\)/\partial x^2$, etc. It is emphasized that the CPT is applied in the remaining of the paper. As a result of this assumption, the Kirchhoff normalcy condition is incorporated, and thus

$$\begin{aligned} \bar{u} &= u - zw_{,x} \\ \bar{v} &= \nu - zw_{,y} \\ \bar{w} &= w \end{aligned} \quad (2)$$

where \bar{u} , \bar{v} and \bar{w} are components of displacement at a general point, whilst u , ν and w are similar

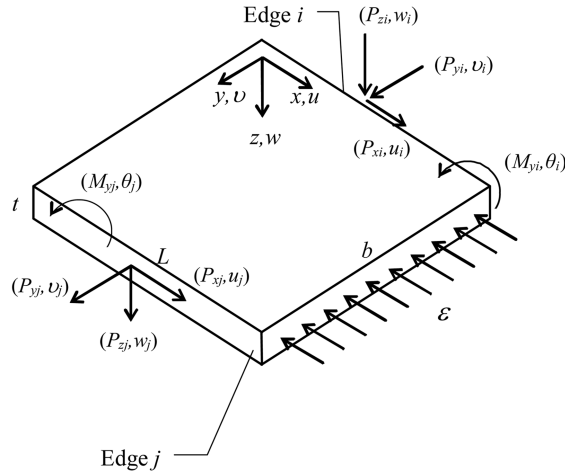


Fig. 1 A typical exact finite strip

components at the middle surfaces ($z = 0$).

On the assumption that the plate is in a state of plane stress, the stress-strain relationship at a general point for the plate becomes

$$\bar{\sigma} = \begin{Bmatrix} \bar{\sigma}_x \\ \bar{\sigma}_y \\ \bar{\tau}_{xy} \end{Bmatrix} = \frac{E}{1-\nu^2} \begin{bmatrix} 1 & \nu & 0 \\ \nu & 1 & 0 \\ 0 & 0 & \frac{1-\nu}{2} \end{bmatrix} \cdot \bar{\epsilon}; \quad \bar{\epsilon} = \begin{Bmatrix} \bar{\epsilon}_x \\ \bar{\epsilon}_y \\ \bar{\gamma}_{xy} \end{Bmatrix} \quad (3)$$

where $\bar{\sigma}$ and $\bar{\epsilon}$, respectively, correspond to the stresses and strains at a general point. Internal forces and moments acting on the edges of a plate/strip are expressed in terms of forces and moments per unit distance along the plate/strip edge. The force and moment intensities are related to the internal stresses by the equations

$$\begin{Bmatrix} \mathbf{N} \\ \mathbf{M} \end{Bmatrix} = \int_{-t/2}^{t/2} \begin{Bmatrix} \bar{\sigma} \\ z\bar{\sigma} \end{Bmatrix} \cdot dz \quad (4)$$

where

$$\mathbf{N} = \begin{Bmatrix} N_x \\ N_y \\ N_{xy} \end{Bmatrix}; \quad \mathbf{M} = \begin{Bmatrix} M_x \\ M_y \\ M_{xy} \end{Bmatrix} \quad (5)$$

In the above equation, N_x, N_y and N_{xy} are the membrane direct and shearing stress resultants per unit length and M_x, M_y and M_{xy} are the bending and twisting stress couples per unit length. It is noted that the stresses and strains in Eq. (3), include the components corresponding to the membrane and bending contributions as outlined below.

$$\bar{\sigma} = \sigma + \sigma_b; \quad \bar{\epsilon} = \epsilon + \epsilon_b \quad (6)$$

Where σ and ϵ correspond to the membrane contribution, and σ_b and ϵ_b relate to the bending and twisting actions. It is noted that the relationship between σ and ϵ is similar to that given by Eq. (3).

The same relationship also applies between σ_b and ϵ_b . Moreover, the membrane strain ϵ can be subdivided into its linear ϵ_l and non-linear ϵ_{nl} components as given below.

$$\epsilon = \epsilon_l + \epsilon_{nl} = \begin{Bmatrix} u_{,x} \\ v_{,y} \\ u_{,y} + v_{,x} \end{Bmatrix} + \begin{Bmatrix} \frac{1}{2}w_{,x}^2 \\ \frac{1}{2}w_{,y}^2 \\ w_{,x}w_{,y} \end{Bmatrix} \quad (7)$$

It is also noted that within the context of CPT the bending strains ϵ_b are expressed by the following equations

$$\epsilon_b = \begin{Bmatrix} -zw_{,xx} \\ -zw_{,yy} \\ -2zw_{,xy} \end{Bmatrix} \quad (8)$$

Since the potential energy of external loads is zero for the plate/strip under consideration, the total potential energy of the plate/strip V_s is simply equal to the its strain energy U_s (i.e., $V_s = U_s$) which is

$$U_s = \frac{1}{2} \iiint (\bar{\sigma}_x \bar{\epsilon}_x + \bar{\sigma}_y \bar{\epsilon}_y + \bar{\tau}_{xy} \bar{\gamma}_{xy}) dx dy dz \quad (9)$$

By substituting $\bar{\sigma}$ and $\bar{\epsilon}$ from Eq. (6) into Eq. (9) and rearranging, the total strain energy of the strip U_s can be expressed by the following equations

$$U_s = U_{ms} + U_{bs} \quad (10)$$

where U_{ms} designates the membrane strain energy of the plate/strip and is given by

$$U_{ms} = \frac{1}{2} \iiint (\sigma_x \epsilon_x + \sigma_y \epsilon_y + \tau_{xy} \gamma_{xy}) dx dy dz \quad (11)$$

and U_{bs} designates the bending strain energy of the plate/strip and is given by

$$U_{bs} = \frac{1}{2} \iiint (\sigma_{bx} \epsilon_{bx} + \sigma_{by} \epsilon_{by} + \tau_{bxy} \gamma_{bxy}) dx dy dz \quad (12)$$

The bending strain energy U_{bs} is expanded by using Eq. (3), and subsequently substituting for ϵ_b by implementing Eq. (8), and finally carrying out the integration in the z direction. This gives

$$U_{bs} = \frac{D}{2} \iint \{ (w_{,xx} + w_{,yy})^2 + 2(1-\nu)(w_{,xy}^2 - w_{,xx}w_{,yy}) \} dx dy \quad (13)$$

where $D = Et^3/12(1-\nu^2)$ is the so-called bending stiffness of the plate/strip.

The von Kármán's equilibrium and compatibility equations for large deflections of plate with the assumption that the normal pressure is zero are given by the following equations respectively.

$$D\nabla^4 w - t(F_{,yy}w_{,xx} - 2F_{,xy}w_{,xy} + F_{,xx}w_{,yy}) = 0 \quad (14-a)$$

$$\nabla^4 F = E(w_{,xy}^2 - w_{,xx}w_{,yy}) \quad (14-b)$$

where $\nabla^4(\cdot) = (\cdot)_{,xxxx} + 2(\cdot)_{,xxyy} + (\cdot)_{,yyyy}$.

In this equation the function F (i.e., $F = F(x, y)$) which is known as the Airy stress function is defined as follows

$$\begin{aligned} F_{,yy} &= \sigma_x = \frac{N_x}{t} \\ F_{,xx} &= \sigma_y = \frac{N_y}{t} \\ F_{,xy} &= -\tau_{xy} = -\frac{N_{xy}}{t} \end{aligned} \quad (15)$$

The membrane strain energy U_{ms} (i.e., Eq. (11)) is further expanded by substituting for ϵ in terms of σ using Eq. (3), and subsequently using Eq. (15) and then carrying out the integration in the z direction. This gives

$$U_{ms} = \frac{t}{2E} \iint \{ (F_{,xx} + F_{,yy})^2 - 2(1 + \nu)(F_{,xx}F_{,yy} - F_{,xy}^2) \} dx dy \quad (16)$$

The positive directions of the edge forces and displacements are shown in Fig. 1. It is noted that the in-plane shear force, in-plane transverse force, out-of-plane shear force and bending moment per unit length of the plate/strip edge are denoted by P_x, P_y, P_z and M_y respectively. The subscripts i and j denote the corresponding values of forces/displacements at edges i and j , respectively. It can be seen in Fig. 1 that the nodal line forces and moments can be expressed in terms of internal in-plane forces and normal displacements on the edges as follows

$$\begin{aligned} P_{xi} &= -N_{xy}|_{y=0}, P_{xj} = N_{xy}|_{y=b} & P_{yi} &= -N_y|_{y=0}, P_{yj} = N_y|_{y=b} \\ P_{zi} &= D[w_{,yyy} + (2 - \nu)w_{,xxy}]_{y=0} & P_{zj} &= -D[w_{,yyy} + (2 - \nu)w_{,xxy}]_{y=b} \\ M_{yi} &= -D[w_{,yy} + \nu w_{,xx}]_{y=0} & M_{yj} &= D[w_{,yy} + \nu w_{,xx}]_{y=b} \end{aligned} \quad (17)$$

In the above equation, as indicated by Wittrick and Williams 1974, the Kirchhoff edge shear force condition has been used for P_z .

By substituting N_y and N_{xy} from Eq. (15) into Eq. (17) for in-plane shear force and in-plane transverse force, P_x and P_y can be expressed as

$$\begin{aligned} P_{xi} &= tF_{,xy}|_{y=0}, P_{xj} = -tF_{,xy}|_{y=b} \\ P_{yi} &= -tF_{,xx}|_{y=0}, P_{yj} = tF_{,xx}|_{y=b} \end{aligned} \quad (18)$$

It is noted that in the remaining of the paper, the subscripts $0,1,2$ are used for pre-buckling, buckling and post-buckling stages, respectively.

2.2 Buckling analysis

The out-of-plane buckling deflection mode w_1 is obtained by trying to solve the Von-Karman's equilibrium equation i.e., Eq. (14-a). This gives

$$D\nabla^4 w_1 - t(F_{0,yy}w_{1,xx} - 2F_{0,xy}w_{1,xy} + F_{0,xx}w_{1,yy}) = 0 \quad (19)$$

where $\nabla^4 w_1 = w_{1,xxxx} + 2w_{1,xyxy} + w_{1,yyyy}$ and F_0 is the Airy stress function in the pre-buckling stage. This equation constitutes a linear eigenvalue problem.

In the pre-buckling stage it is assumed that the plate/strip is subjected to the compressive axial stress and thus

$$\sigma_{x0} = -\sigma, \quad \sigma_{y0} = 0, \quad \sigma_{xy0} = 0 \quad (20)$$

where $\sigma = E\varepsilon$ and ε is the end-shortening strain in the pre-buckling stage. Then by using Eq. (15)

$$F_{0,yy} = -\sigma, \quad F_{0,xx} = 0, \quad F_{0,xy} = 0 \quad (21)$$

By substituting Eq. (21) into Eq. (19), the Von-Karman's equilibrium equation in the buckling analysis can be expressed by the following form

$$D(w_{1,xxxx} + 2w_{1,xyxy} + w_{1,yyyy}) + t\sigma w_{1,xx} = 0 \quad (22)$$

A Separable form is assumed for the displacement w_1 in order to reduce the above partial differential equation into an ordinary differential equation. The out-of-plane buckling deflection mode w_1 is assumed to vary sinusoidally with x . This assumption is consistent with the boundary conditions set forth earlier by the Eq. (1). Thus, the out-of-plane buckling deflection mode w_1 is

$$w_1(x, y) = f_{w_1}(y) \cdot \sin(\lambda x) \quad (23)$$

where $\lambda = n\pi/L$ and parameter n in the above displacement function is merely an integer which represents the number of buckle half-wavelengths along the strip, and $f_{w_1}(y)$ represents the shape function in the transverse direction y . Substituting out-of-plane buckling deflection mode w_1 from Eq. (23) into Eq. (22) and rearranging leads to the following fourth-order ordinary differential equation

$$f_{w_1}'''' - 2\lambda^2 f_{w_1}'' + \lambda^4(1 - \zeta)f_{w_1} = 0 \quad (24)$$

where $\zeta = \sigma t/\lambda^2 D$, and the superscript ' ' denotes differentiation with respect to y , i.e., $()' = d()/dy$. The solution of Eq. (24) depends on whether ζ , which is clearly positive, is greater than, less than, or equal to unity, thus

For $\zeta > 1$, the solution can be written as

$$f_{w_1}(y) = C_{w_1}^{(1)} \cosh(\alpha\lambda y) + C_{w_1}^{(2)} \sinh(\alpha\lambda y) + C_{w_1}^{(3)} \cos(\beta\lambda y) + C_{w_1}^{(4)} \sin(\beta\lambda y) \\ \alpha = \sqrt{1 + \sqrt{\zeta}} \quad \beta = \sqrt{-1 + \sqrt{\zeta}} \quad (25)$$

while for $0 < \zeta < 1$

$$f_{w_1}(y) = C_{w_1}^{(1)} \cosh(\alpha\lambda y) + C_{w_1}^{(2)} \sinh(\alpha\lambda y) + C_{w_1}^{(3)} \cosh(\beta\lambda y) + C_{w_1}^{(4)} \sinh(\beta\lambda y) \\ \alpha = \sqrt{1 + \sqrt{\zeta}} \quad \beta = \sqrt{1 - \sqrt{\zeta}} \quad (26)$$

and for $\zeta = 1$

$$f_{w_1}(y) = C_{w_1}^{(1)} \cosh(\sqrt{2}\lambda y) + C_{w_1}^{(2)} \sinh(\sqrt{2}\lambda y) + C_{w_1}^{(3)} y + C_{w_1}^{(4)} \quad (27)$$

where $C_{w_1}^{(k)}$ ($k = 1, 2, 3, 4$) denote unknown constants. However, in practical situations, only the case $\zeta > 1$ has ever been encountered by the authors. Therefore, the associated computer program has no coding for the cases $0 < \zeta < 1$ and $\zeta = 1$ and would simply print a message if such cases were ever detected. The displacement boundary conditions for $f_{w_1}(y)$ at the two edges $y = 0$ and $y = b$ can be written as

$$\begin{aligned} f_{w_1}(0) &= w_{1i}, & f_{w_1}(b) &= w_{1j} \\ f'_{w_1}(0) &= \theta_{1i}, & f'_{w_1}(b) &= \theta_{1j} \end{aligned} \quad (28)$$

where the subscript 1 is used because they are initial buckling quantities and the subscripts i and j denote amplitudes at edges i and j of the strip, respectively. These buckling displacement amplitudes, which are depicted in Fig. 1, can be written as the displacement vector

$$\underline{\mathbf{d}}_1 = \{w_{1i}, \theta_{1i}, w_{1j}, \theta_{1j}\}^T \quad (29)$$

The four unknown constants $C_{w_1}^{(k)}$ ($k = 1, 2, 3, 4$) corresponding to a given plate/strip can be fully determined in terms of buckling displacement amplitudes by substituting the boundary conditions of Eq. (28) into Eq. (25). Thus, the solution of fourth-order ordinary differential Eq. (24) which satisfies the displacement boundary conditions of Eq. (28) can be obtained analytically in terms of the edge displacements $\underline{\mathbf{d}}_1$. Substituting Eq. (23) into Eq. (17) yields the force boundary conditions for the moment and out-of-plane edge shear force as

$$\begin{aligned} P_{1zi} &= D[f''_{w_1}(0) - (2 - \nu)\lambda^2 \theta_{1i}], & P_{1zj} &= -D[f''_{w_1}(b) - (2 - \nu)\lambda^2 \theta_{1j}] \\ M_{1yi} &= -D[f''_{w_1}(0) - \nu\lambda^2 w_{1i}], & M_{1yj} &= D[f''_{w_1}(b) - \nu\lambda^2 w_{1j}] \end{aligned} \quad (30)$$

The left-hand sides of Eq. (30) are the amplitudes of the buckling forces and moments at the corresponding edges of the plate/strip. They can be written as the force vector

$$\underline{\mathbf{p}}_1 = \{P_{1zi}, M_{1yi}, P_{1zj}, M_{1yj}\}^T \quad (31)$$

The above equation which describes the edge forces in terms of the edge displacements can be rearranged as

$$\underline{\mathbf{p}}_1 = \underline{\mathbf{k}}_1 \underline{\mathbf{d}}_1 \quad (32)$$

Where $\underline{\mathbf{k}}_1$ denotes the plate out-of-plane stiffness matrix. By applying these expressions to obtain the stiffness matrices of individual strips, the exact overall stiffness matrix $\underline{\mathbf{K}}_1$ for the whole plate can be assembled by using the conventional routines of finite element analysis. The corresponding buckling problem can finally be expressed as the eigenvalue problem

$$\underline{\mathbf{K}}_1(\sigma) \underline{\mathbf{D}}_1 = 0 \quad (33)$$

Where the vector $\underline{\mathbf{D}}_1$ consists of the out-of-plane displacement amplitudes (w_1, θ_1) for each nodal line, and $\underline{\mathbf{K}}_1$ is the stiffness matrix whose coefficients include trigonometric and hyperbolic functions involving longitudinal stress σ as the plate/strip is analyzed exactly by solving its

governing differential equation.

It is realized that the application of the exact method for buckling of structures has resulted in a transcendental eigenvalue problem in the form of Eq. (33) as distinct from equation $(\mathbf{K} - \sigma \mathbf{K}_G) \mathbf{D} = 0$ which is encountered when approximate methods such as finite strip method are used.

Such exact analyses always lead to considerable reductions in the order of $\mathbf{K}_1(\sigma)$ compared to that required in the case of approximate analyses.

There are many well-established and excellent alternative methods for solving the generalized linear eigenvalue problem to find both the eigenvalues and eigenvectors, i.e., the critical longitudinal stress and buckling modes, accurately and with complete certainty that none is missed, Wilkinson 1965 and Bathe 1996. However these methods are not directly applicable to the transcendental eigenvalue problem in the form of Eq. (33). In the case of transcendental eigenvalue problem, in the first stage it is necessary to implement a special algorithm, which has been developed by Wittrick-Williams (W-W), in order to calculate the number of eigenvalues (critical stresses) exceeded by any trial value of σ . The use of the W-W algorithm is essential as otherwise there will certainly be structures for which some of the eigenvalues will be missed.

Having calculated the number of eigenvalues, certain methods for finding the eigenvalue and eigenvector of the transcendental eigenvalue problem can be used. The details of the W-W algorithm and the two secure methods for finding the eigenvalue and eigenvector of the transcendental eigenvalue problem are presented below. The first method utilizes a bisection method, Wittrick and Williams 1974, whereas in the second method (which is designated by the name recursive Newton method) transcendental eigenvalue problem is first reduced to a generalized linear eigenvalue problem by using Newton's method in the vicinity of an exact critical stress, Yuan *et al.* 2003. Then the generalized linear eigenvalue problem is effectively solved by using a standard inverse iteration method.

It is noted that in the remainder of the paper the critical stresses of any strip with both longitudinal edges clamped are denoted by σ_{Cb} , which is to be called strip clamped-edge stresses.

2.2.1 Wittrick-Williams algorithm

The W-W algorithm, Wittrick and Williams 1970-1973, is a theoretically proven, reliable and efficient tool to obtain the number of eigenvalues (i.e., critical load factors in the buckling problems or natural frequencies in the free vibration studies) of transcendental eigenvalue equations to any required accuracy. The algorithm does not directly compute the eigenvalues, but instead simply finds J , the total number of eigenvalues below an arbitrarily given trial value. In this way the upper and lower bounds are established on each required eigenvalue, after which various iterative procedures can be used to converge on the eigenvalue to the required accuracy.

Let $J(\sigma_i)$ be the number of (positive) eigenvalues (critical stresses) which are less than some chosen (positive) value σ_i , a trial value of σ , as

$$J(\sigma_i) = J_0(\sigma_i) + sg\{\mathbf{K}_1(\sigma_i)\} \quad (34)$$

where

$$J_0(\sigma_i) = \sum_s J_s(\sigma_i) \quad (35)$$

where the summation is over all strips in a plate (if required) and $J_s(\sigma_i)$ is the number of strip clamped-edge stresses σ_{CI} that are less than chosen value σ_i (for each strip). It is noted that J_s can be calculated from simple formulae for most commonly used plates, or otherwise numerical procedures are available for its calculation, Wittrick and Williams 1974. Finally, $sg\{\mathbf{K}_1(\sigma_i)\}$ is known as the ‘sign count’ of $\mathbf{K}_1(\sigma_i)$ and can be calculated as the number of negative leading diagonal elements of $\mathbf{K}_1^A(\sigma_i)$, the upper triangular matrix obtained from $\mathbf{K}_1(\sigma_i)$ by the usual form of Gauss elimination, without row interchanges, scaling or pivoting.

Clearly σ_i corresponds to a lower bound value (i.e., σ_L) on the r th critical stresses if $J(\sigma_i) < r$, and otherwise σ_i is an upper bound (i.e., σ_U). Hence the numbers of critical stresses N_r and strip clamped-edge stresses N_{r0} lying in the interval (σ_L, σ_U) are given by

$$N_r = J(\sigma_U) - J(\sigma_L), \quad N_{r0} = J_0(\sigma_U) - J_0(\sigma_L) \quad (36)$$

2.2.2 Bisection method

The outcome of Eq. (34) has allowed the authors to calculate the number of positive critical stresses which lie below any chosen value of σ_i . In this way, it is not difficult to devise an automatic procedure by using Eq. (34) for finding two values σ_U and σ_L which provide upper and lower bounds to σ_r , which is the r th eigenvalue. This knowledge eliminates entirely the need to increment σ in very small steps in seeking the eigenvalues of Eq. (33) and lends itself admirably to an iterative computational procedure such as the well-known bisection convergence method for converging upon any required eigenvalues. The bisection convergence method has the advantage that it converges to the eigenvalues with certainty and with any specified degree of accuracy. Once a pair of upper and lower bounds have been established, the bisection method requires the interval between the bounds to be progressively narrowed according to the simple Eq. (37). Having obtained the new value of σ based on Eq. (37), the Eq. (34) is then implemented to find out whether the obtained σ is an improved upper bound or an improved lower bound.

$$\sigma = \frac{1}{2}(\sigma_U + \sigma_L) \quad (37)$$

This bisection step is repeated until upper and lower bounds differ by less than the user specified error tolerance $Tol1$. This paper adopts the termination criterion as

$$\sigma_U - \sigma_L \leq Tol1 \quad (38)$$

Each iteration halves the interval so that 10 iterations improve the accuracy approximately 1000 times (2^{10}).

The main disadvantage of the bisection method is that it does not provide the eigenvectors, whose knowledge is often necessary in a thorough buckling study. Therefore, an extension of the method is provided in the developed computer program in order to calculate the pertinent eigenvectors.

2.2.3 Recursive newton method

The theoretical development of the recursive Newton method for solving the transcendental eigenvalue problems in the current study is essentially similar to the approach adopted by Yuan *et al.* 2003.

Suppose a stress interval (σ_L, σ_U) has been identified by the W-W algorithm or by some other

means, and it has been determined that there is only one critical stress σ_g and no strip clamped-edge stresses σ_{Cl} inside the interval, i.e., $N_r = 1$ and $N_{r0} = 0$. Let σ_a denote the best available approximation to the exact critical stress σ_g in (σ_L, σ_U) . Initially σ_a is set to be at the middle of the interval, i.e., $\sigma_a = \frac{1}{2}(\sigma_L + \sigma_U)$, to ensure that its nearest critical stress is the one within (σ_L, σ_U) . Moreover, let the following notation be introduced

$$\tilde{\mathbf{K}}_{1g} = \tilde{\mathbf{K}}_1(\sigma_g), \quad \tilde{\mathbf{K}}_{1a} = \tilde{\mathbf{K}}_1(\sigma_a), \quad \tilde{\mathbf{K}}'_{1a} = \frac{d\tilde{\mathbf{K}}_1(\sigma_a)}{d\sigma}, \quad \tilde{\mathbf{K}}''_{1a} = \frac{d^2\tilde{\mathbf{K}}_1(\sigma_a)}{d\sigma^2} \quad (39)$$

Here, $\tilde{\mathbf{K}}'_{1a}$ and $\tilde{\mathbf{K}}''_{1a}$ are assembled from first and second derivatives of the strip stiffness matrices, respectively.

Consider the Taylor series expansion

$$\tilde{\mathbf{K}}_{1g} = \tilde{\mathbf{K}}_{1a} + (\sigma_g - \sigma_a)\tilde{\mathbf{K}}'_{1a} + \frac{(\sigma_g - \sigma_a)^2}{2}\tilde{\mathbf{K}}''_{1a} + O((\sigma_g - \sigma_a)^3) \quad (40)$$

Right multiplication by the exact mode vector $\tilde{\mathbf{D}}_{1g}$ leads to

$$\tilde{\mathbf{K}}_{1g}\tilde{\mathbf{D}}_{1g} = \tilde{\mathbf{K}}_{1a}\tilde{\mathbf{D}}_{1g} + (\sigma_g - \sigma_a)\tilde{\mathbf{K}}'_{1a}\tilde{\mathbf{D}}_{1g} + \frac{(\sigma_g - \sigma_a)^2}{2}\tilde{\mathbf{K}}''_{1a}\tilde{\mathbf{D}}_{1g} + O((\sigma_g - \sigma_a)^3) \quad (41)$$

Nothing that $\tilde{\mathbf{K}}_{1g}\tilde{\mathbf{D}}_{1g} = 0$ and ignoring the second and higher order terms yields

$$\tilde{\mathbf{K}}_{1a}\tilde{\mathbf{D}}_{1g} = (\sigma_g - \sigma_a)\tilde{\mathbf{K}}'_{1a}\tilde{\mathbf{D}}_{1g} \quad (42)$$

Eq. (42) implies that with an approximate σ_a , $\tilde{\mathbf{K}}_{1a}$ and $\tilde{\mathbf{K}}'_{1a}$ known, a better approximation to the exact critical stress σ_a and mode vector $\tilde{\mathbf{D}}_{1g}$ can be obtained by solving the generalized linear eigenvalue problem

$$\tilde{\mathbf{K}}_{1a}\tilde{\mathbf{D}}_1 = \mu\tilde{\mathbf{K}}'_{1a}\tilde{\mathbf{D}}_1 \quad (43)$$

It is noted that $\tilde{\mathbf{K}}'_{1a}$ is derived analytically in the current study. Eq. (43) is a typical formulation of Newton's method, which represents a linearization of the original transcendental problem $\tilde{\mathbf{K}}_{1g}\tilde{\mathbf{D}}_{1g} = 0$ in the vicinity of σ_g . After obtaining the solution of Eq. (43), i.e., the eigenvalue μ and the associated eigenvector $\tilde{\mathbf{D}}_1$, a possibly more accurate stress can be extrapolated by

$$\sigma_\mu = \sigma_a - \mu \quad (44)$$

It is well known that if σ_a is sufficiently close to σ_g , Newton's method has second order accuracy (i.e., of the order of $(\sigma_g - \sigma_a)$ for a single σ_g ($N_r = 1$)). The second order accuracy implies that, in order to obtain a final approximate stress satisfying the error tolerance $Tol1$ in the way defined by Eq. (38), it suffices to narrow the stress interval until $\sigma_U - \sigma_L \leq \sqrt{Tol1}$. Then one iteration of Newton's solution will give both stress and mode vector with the accuracy approximately satisfying the required tolerance $Tol1$.

In the present study the inverse iteration procedure, which is employed by Yuan *et al.* 2003, is selected for solving the Eq. (43).

Solving Eq. (43) involves many eigenpairs but, because $N_r = 1$, only one of them satisfies $\sigma_L < \sigma_\mu < \sigma_U$. A natural method that is guaranteed to converge on the eigenpair for which the

absolute eigenvalue μ is least is the inverse iteration procedure, which is employed in this paper and the Rayleigh quotient is used to accelerate the convergence on the eigenvalues, giving

$$\begin{aligned} \bar{\mathbf{D}}_1^{(\gamma+1)} &= \mathbf{K}_{1a}^{-1} \mathbf{K}'_{1a} \mathbf{D}_1^{(\gamma)} \text{ with } \mathbf{D}_1^{(0)} \text{ a random vector} \\ \mu^{(\gamma+1)} &= \frac{\bar{\mathbf{D}}_1^{(\gamma+1)T} \mathbf{K}_{1a} \bar{\mathbf{D}}_1^{(\gamma+1)}}{\|\bar{\mathbf{D}}_1^{(\gamma+1)}\|^2} \text{ with } \|\bar{\mathbf{D}}_1^{(\gamma+1)}\|^2 = \bar{\mathbf{D}}_1^{(\gamma+1)T} \mathbf{K}'_{1a} \bar{\mathbf{D}}_1^{(\gamma+1)} \\ \mathbf{D}_1^{(\gamma+1)} &= \frac{\bar{\mathbf{D}}_1^{(\gamma+1)}}{\bar{D}_{1m^*}^{(\gamma+1)}} \text{ with } \bar{D}_{1m^*}^{(\gamma+1)} = \max|\bar{D}_{1m}^{(\gamma+1)}| \end{aligned} \quad (45)$$

which is terminated when

$$|\mu^{(\gamma+1)} - \mu^{(\gamma)}| < Tol2 \quad (46)$$

where $D_{1m}^{(\gamma)}$ is m th element of $\mathbf{D}_1^{(\gamma)}$; max denotes the maximum value for any m , and $Tol2$ is the user specified error tolerance, which may or may not be equal to $Tol1$ in Eq. (38). It can be seen that at each iteration of the Newton method, the solution for the eigenvalue μ and the associated eigenvector \mathbf{D}_1 is achieved by the inverse iteration method. It is noted that for some initial values of σ_a , it is likely that the Newton's method converge to the solution σ_μ which may not lie within (σ_L, σ_U) . Therefore, it is necessary to carry out the so-called μ -check, which means checking whether σ_μ lies within (σ_L, σ_U) .

Having calculated a μ value which satisfies the error criterion of Eq. (46), a better approximation to σ_μ is calculated using Eq. (44) and a μ -check is performed to see if the results are acceptable. If so, σ_a is replaced by σ_μ and the inverse iteration procedure is carried out to obtain better approximations for the stresses and mode vectors. This procedure is repeated until σ_μ and σ_a differ by less than the user specified error tolerance $Tol3$, i.e., $\mu < Tol3$.

It is emphasized that the solution of Eq. (33) in the manner described above leads to the buckling stress σ and the corresponding out-of-plane buckling deflection mode w_1 for each plate/strip.

2.3 Post-buckling analysis

Generally, in a multi-term post-buckling analysis, each of the in-plane or out-of-plane displacements can be postulated by a summation of displacement functions, each of which being multiplied by an unknown coefficient. It is noted that each of the assumed displacement functions is required to satisfy the corresponding in-plane or out-of-plane boundary conditions. In the current paper, however, since the objective is to investigate the initial post-buckling behaviour of the plate, a single-term approach is considered to be appropriate. It is assumed that the deflected form immediately after the buckling is the same as that obtained for the buckling. Thus, the out-of-plane buckling deflection mode, corresponding to the lowest buckling load, i.e., the first mode, is used for the initial post-buckling study. Moreover, it is noted that as far as the in-plane displacements are concerned, their functions are obtained by solving the Von-Karman's compatibility equation governing the behavior of isotropic flat plates.

Having obtained an exact shape of the deflected form at buckling from the buckling analysis, the analysis of post-buckling behavior can proceed on the assumption that the deflected form in the

immediate post-buckling range is identical to that at buckling, with only the deflection magnitudes varying. Thus, the post-buckling out-of-plane deflection function w_2 can be written as

$$w_2(x, y) = \delta \cdot w_1(x, y) \quad (47)$$

where δ is the deflection coefficient. The stresses occurring in the plate after the buckling are related to the deflection of the plate via the Von-Karman's compatibility equation i.e., Eq. (14-b).

$$\nabla^4 F_2 = E(w_{2,xy}^2 - w_{2,xx}w_{2,yy}) \quad (48)$$

Substituting Eq. (23) and (47) into Eq. (48) yields

$$\nabla^4 F_2 = \frac{E\lambda^2\delta^2}{2} [(f'_{w1})^2 + f_{w1}f''_{w1} + [(f'_{w1})^2 - (f_{w1}f''_{w1})] \cos(2\lambda x)] \quad (49)$$

The above equation indicates that the stress function F_2 may be considered in two parts: one part is constant with respect to x , and the other part is varying periodically with x , i.e.

$$F_2(x, y) = F_{20}(y) + F_{22}(y) \cos(2\lambda x) \quad (50)$$

The plate/strip is assumed to be subjected to an in-plane compressive loading acting through frictionless rigid platens in the post-buckling region such that uniform end-shortening strain ε occurs at end $x = L$ only (see Fig. 1). The in-plane boundary conditions at loaded ends of the plate/strip are summarized as follows

$$N_{xy} = 0 \quad \text{at} \quad x = 0 \& L, \quad u_2 = \begin{cases} 0 & x = 0 \\ -\varepsilon L & x = L \end{cases} \quad (51)$$

By substituting F_2 from Eq. (50) in Eq. (49) whilst imposing the boundary conditions as Eq. (51), and following the semi-energy post-buckling procedure in the manner described in Ref. Ovesy *et al.* 2004, F_{20}'' and the post-buckling in-plane u_2 displacement function corresponding to the out-of-plane buckling deflection mode and the deflection coefficient δ can eventually be derived as Eqs. (52) and (53), respectively.

$$F_{20}'' = -E\varepsilon + \frac{E\lambda^2\delta^2}{4} f_{w1}^2 \quad (52)$$

$$u_2(x, y) = -\varepsilon x + \delta^2 f_{u2}(y) \sin(2\lambda x) \quad (53)$$

where

$$f_{u2}(y) = f_{u2} = \frac{\lambda}{4} \left(\psi'' + 4\nu\lambda^2 \psi - \frac{f_{w1}^2}{2} \right) \quad (54)$$

and $\psi = \psi(y)$ can be found from the following equation

$$\psi'''' - 8\lambda^2 \psi'' + 16\lambda^4 \psi = (f'_{w1})^2 - f_{w1}f''_{w1} \quad (55)$$

where

$$F_{22}(y) = \frac{E\lambda^2\delta^2}{2}\psi(y) \tag{56}$$

It is noted that the first term on the right hand side of Eq. (53) represents the prescribed uniform end-shortening strain. The amplitude of the second term whilst divided by δ^2 and evaluated at $y = 0$ and $y = b$ (i.e., $f_{u2}|_{y=0}, f_{u2}|_{y=b}$) represents the post-buckling in-plane displacement parameters u_{2i} and u_{2j} respectively (see Fig. 1). It is also noted that the post-buckling in-plane u_2 displacement is a function of out-of-plane buckling deflection mode (which is a function of critical longitudinal stress) and deflection coefficient δ .

The solution of Eq. (55) is composed of two parts; the particular integral solution $\psi_{P,I}$, and the general solution ψ_G .

$$\psi = \psi_{P,I} + \psi_G \tag{57}$$

Having known the out-of-plane buckling mode shape, i.e., f_{w1} in the buckling analysis, f_{w1} and its derivatives are substituted in the right-hand side of Eq. (55) so that it changes to the following form

$$(C^{(1)}\sin(\beta\lambda y) + C^{(2)}\cos(\beta\lambda y))\sinh(\alpha\lambda y) + (C^{(3)}\sin(\beta\lambda y) + C^{(4)}\cos(\beta\lambda y))\cosh(\alpha\lambda y) + C^{(5)} \tag{58}$$

where $C^{(k)}(k = 1 \dots 5)$ are known constant. The particular integral solution $\psi_{P,I}$, which depends on the out-of-plane buckling deflection mode, takes the same form as expression (58), and can be found by using the method of undetermined coefficients.

The general solution ψ_G is as follows

$$\psi_G(y) = C_{\psi}^{(1)}\sinh(2\lambda y) + C_{\psi}^{(2)}\cosh(2\lambda y) + C_{\psi}^{(3)}y\sinh(2\lambda y) + C_{\psi}^{(4)}y\cosh(2\lambda y) \tag{59}$$

The coefficients $C_{\psi}^{(k)}(k = 1, 2, 3, 4)$ are unknown at present, but it is assumed that these coefficients and subsequently ψ_G and ψ are known so that the analysis to find the in-plane displacements can be completed.

The post-buckling in-plane v_2 displacement can be developed in the same manner as that described in Ovesy *et al.* (2004) with respect to the semi-energy post-buckling finite strip.

$$v_2 = v\epsilon y + \delta^2(I_{1v_2}(y) + f_{v2}(y)\cos(2\lambda x) - f_{v2}(y)|_{y=0}) + v|_{x=y=0} \tag{60}$$

where

$$I_{1v_2}(y) = -\int_0^y \left(\frac{4\nu\lambda^2}{16}f_{w1}^2 + \frac{(f'_{w1})^2}{4} \right) \tag{61}$$

$$f_{v2}(y) = f_{v2} = \frac{1}{8}(\psi''' - 4(2 + \nu)\lambda^2\psi' + f_{w1}f'_{w1})$$

The above equation describes the in-plane v_2 displacement function corresponding to the out-of-plane buckling deflection mode (which is determined in the buckling analysis) and deflection coefficient δ .

The first term on the right hand side of Eq. (60) describes the transverse in-plane expansion of the plate/strip, which occurs due to the Poisson's ratio effect. The second term (i.e., $\delta^2 I_{1v_2}(y)$)

describes the transverse in-plane movement of the longitudinal fibers of the plate/strip. This movement, which is constant along the length of a given fiber, varies from a minimum value of zero at edge $y = 0$ to its maximum value at the edge $y = b$. The third term describes the in-plane waviness of the longitudinal fibers. The amplitude of this term whilst divided by δ^2 and evaluated at $y = 0$ and $y = b$ (i.e., $f_{v_2}|_{y=0}, f_{v_2}|_{y=b}$) represents the post-buckling in-plane displacement parameters v_{2i} and v_{2j} respectively (see Fig. 1). Finally, the fourth term (which is equivalent to $\delta^2 v_{2i}$) and the fifth term on the right hand side of Eq. (60) represent values which remain constant at all points on a given plate/strip. The existence of the fourth term on the right hand side of Eq. (60) (i.e., $-\delta^2 f_{v_2}|_{y=0} = -\delta^2 v_{2i}$) allows the point $(x = 0, y = 0)$ to be treated as a reference point in terms of its deflection being connected to another strip or being restrained. The obtained expression for the in-plane v_2 displacement function (i.e., Eq. (60)) clearly shows that by setting v_{2i} or v_{2j} equal to 0, only the in-plane waviness of the corresponding edge is prevented (i.e., the corresponding edge is kept straight) but the edge is still allowed to move.

It is noted that the post-buckling in-plane displacement amplitudes (i.e., u_{2i}, u_{2j}, v_{2i} and v_{2j}) can explicitly be described in terms of the four unknown coefficients $C_{\psi}^{(k)}$ ($k = 1, 2, 3, 4$). The four equations describing $u_{2i}, u_{2j}, v_{2i}, v_{2j}$ are then solved by treating the coefficients $C_{\psi}^{(k)}$ ($k = 1, 2, 3, 4$) as unknowns, while all other parameters, including all in-plane post-buckling displacement amplitudes (i.e., $u_{2i}, u_{2j}, v_{2i}, v_{2j}$) are assumed to be known. Thus, the coefficients $C_{\psi}^{(k)}$ ($k = 1, 2, 3, 4$) are explicitly described in terms of $u_{2i}, u_{2j}, v_{2i}, v_{2j}, b, \lambda, v$. Having found the coefficients $C_{\psi}^{(k)}$ ($k = 1, 2, 3, 4$), they are substituted in Eq. (59) to find the general solution. Subsequently, the combination of the general and particular integral solutions is used to substitute for ψ in the expression describing F_{22} (i.e., Eq. (56)).

By substituting the stress function F_2 from Eq. (50) into Eq. (18) for in-plane shear force and in-plane transverse force, amplitudes of P_x and P_y in the post-buckling region can be expressed by the following equations

$$\begin{aligned} P_{2xi} &= -2t\lambda F'_{22}|_{y=0}, & P_{2xj} &= 2t\lambda F'_{22}|_{y=b} \\ P_{2yi} &= 4t\lambda^2 F_{22}|_{y=0}, & P_{2yj} &= -4t\lambda^2 F_{22}|_{y=b} \end{aligned} \quad (62)$$

The in-plane shear force and in-plane transverse force obtained from Eq. (62) are composed of two parts; one part which corresponds to the particular integral solution $\psi_{p,I}$ is a function of the out-of-plane displacement parameters (buckling displacement amplitudes w_1, θ_1), and the other part which corresponds to the general solution ψ_G , is a function of the in-plane displacement parameters (i.e., u_2, v_2).

Eq. (62) can be re-arranged to obtain the following set of linear simultaneous equations for the strip, which is designated as the strip stiffness equations.

$$\underline{\mathbf{p}}_2 = \underline{\mathbf{k}}_2 \underline{\mathbf{d}}_2 + \underline{\mathbf{f}}_2 \quad (63)$$

Where

$$\underline{\mathbf{d}}_2 = \{u_{2i}, v_{2i}, u_{2j}, v_{2j}\}^T \quad (64)$$

and

$$\underline{\mathbf{p}}_2 = \{P_{2xi}, P_{2yi}, P_{2xj}, P_{2yj}\}^T \quad (65)$$

Whilst $\underline{\underline{f}}_2$ consists of terms which correspond to the particular integral solution $\psi_{p,l}$, and $\underline{\underline{k}}_2$ is the stiffness matrix of the strip.

Having developed the stiffness equations for each strip (i.e., Eq. (63)), the overall stiffness equations corresponding to the whole plate are formed by following the conventional finite element assembly procedure, and noting that the plate is not subjected to any external force, thus $\underline{\underline{p}}_2$ vectors vanishes during assembly process. The overall stiffness equations are

$$\underline{\underline{K}}_2 \underline{\underline{D}}_2 = \underline{\underline{F}}_2 \tag{66}$$

Where matrices $\underline{\underline{K}}_2$, $\underline{\underline{D}}_2$ and $\underline{\underline{F}}_2$ are assembled from their counterparts (i.e., $\underline{\underline{k}}_2$, $\underline{\underline{d}}_2$ and $\underline{\underline{f}}_2$) for each strip. Once Eq. (66) is solved and the post-buckling in-plane displacement parameters (i.e., $u_{2i}, u_{2j}, v_{2i}, v_{2j}$) are obtained, they are then substituted into Eq. (53) and (60) to determine the analytical form of u_2 and v_2 for each strip, respectively. It is noted that the obtained u_2, v_2 and the assumed w_2 are all determined in terms of the deflection coefficient δ , which will be calculated below.

2.4 Deflection coefficient (δ) calculation

As described in subsection Basic formulation of the problem, for a prescribed uniform end-shortening strain ε , the strain energy of the strip U_s which is simply equal to its total potential energy V_s , is composed of bending strain energy U_{bs} and membrane strain energy, U_{ms} (i.e., Eq. (10)). Substitution of Eqs. (47), (50), (52) and (56) into Eq. (13) and (16), and summation of all strip energies give

$$U_m = \delta^4 m_4 - \delta^2 \varepsilon m_2 + \varepsilon^2 m_0 \quad U_b = \delta^2 b_2 \tag{67}$$

where U_m and U_b are the membrane and bending strain energies of the plate, respectively, and

$$\begin{aligned} m_4 &= \sum \left\{ \left(\frac{1}{32} tEL\lambda^4 \int_0^b (32\lambda^4 \psi^2 + 16\lambda^2 \psi'^2 + 2\psi''^2 + f_{w1}^4) dy \right) + \frac{1}{2} tEL\lambda^6 v(\psi\psi') \Big|_0^b \right\} \\ m_2 &= \sum \frac{1}{4} tEL\lambda^2 \int_0^b f_{w1}^2 dy \\ m_0 &= \sum \frac{1}{2} tELb \end{aligned} \tag{68}$$

$$b_2 = \sum \left\{ \left(\frac{1}{4} LD \int_0^b (f_{w1}''^2 - 2\lambda^2 f_{w1}'^2 + \lambda^4 f_{w1}^2 - 4\lambda^2 f_{w1} f_{w1}'') dy \right) + \frac{1}{2} LD\lambda^2 v(f_{w1} f_{w1}'') \Big|_0^b \right\}$$

Here the summation \sum relates to all strips. For a prescribed post-buckling end-shortening strain ε , the above constants can be obtained by substituting the functions $f_{w1}(y)$ and ψ from Eqs. (25) and (57) respectively into their integrands and carrying out the integration analytically. It is emphasized that these constants need to be evaluated only once. It is noted that the deflection coefficient δ is the only unknown in the energy expression. The strain energy is then minimized by differentiating U with respect to δ . This gives

$$\frac{dU}{d\delta} = 4m_4\delta^3 + 2(-m_2\varepsilon + b_2)\delta = 0 \quad (69)$$

where $U = U_m + U_b$. It is noted that in the above equation $\delta = 0$ relates to the trivial equilibrium path, and thus the branched equilibrium path is obtained by dividing the above equation by δ to give

$$4m_4\delta^2 + 2(-m_2\varepsilon + b_2) = 0$$

$$\delta = \pm \sqrt{\frac{m_2\varepsilon - b_2}{2m_4}} \quad (70)$$

In Eq. (70), since m_2, b_2 and m_4 are all known constants, δ can be solved for any prescribed value of end-shortening strain ε . The obtained expression for the deflection coefficient δ clearly shows that the critical end-shortening strain ε_{Cr} and the corresponding buckling stress (i.e., $\sigma_{Cr} = E\varepsilon_{Cr}$) can alternatively be obtained by setting δ equal to 0. This buckling stress (i.e., $\sigma_{Cr} = Eb_2/m_2$) is identical to that obtained earlier in connection with the buckling study of the plate. It is noted that for $\varepsilon < \varepsilon_{Cr}$ the value of δ is imaginary.

The longitudinal mid-plane stress σ_x is defined by the following equation, which is obtained from Eqs. (15), (50), (52) and (56).

$$\sigma_x = -E\varepsilon + \frac{E\lambda^2\delta^2}{4}(f_{w1}^2 + 2\psi''\cos(2\lambda x)) \quad (71)$$

The longitudinal force/load acting on a strip is determined by integrating the longitudinal mid-plane stresses σ_x over the strip cross-sectional area, i.e.

$$P_s = E\varepsilon bt - \frac{Et\lambda^2\delta^2 b}{4} \int_0^b (f_{w1}^2 + 2\psi''\cos(2\lambda x)) dy \quad (72)$$

It is seen that the above equation is multiplied by a negative sign, so that positive P_s values represent compression forces. The total longitudinal force/load acting on a plate at a given cross section along the plate length, corresponding to a prescribed end-shortening strain, is obtained by summation of all strip forces P_s at the same cross section, i.e.

$$P = \sum P_s = E\varepsilon t \sum b - \frac{Et\lambda^2\delta^2}{4} \sum \int_0^b (f_{w1}^2 + 2\psi''\cos(2\lambda x)) dy \quad (73)$$

By substituting the deflection coefficient δ from Eq. (70) into Eq. (73) and rearranging

$$P = Et\varepsilon \left(\sum b - \frac{\lambda^2 m_2}{8m_4} \sum \int_0^b (f_{w1}^2 + 2\psi''\cos(2\lambda x)) dy \right)$$

$$+ Et \frac{\lambda^2 b_2}{8m_4} \sum \int_0^b (f_{w1}^2 + 2\psi''\cos(2\lambda x)) dy \quad (74)$$

It is seen that the P - ε relationship in the post-buckling region is a linear function which is tangent to the actual post-buckling curve at the buckling point. The slope of this line, which is post-buckling stiffness S^* , can be obtained by differentiating Eq. (74) with respect to ε . The effective pre-

buckling stiffness S can be obtained by letting $\delta = 0$ in Eq. (73) and differentiating the equation with respect to ε . Therefore, the relative post-buckling stiffness defined as the ratio of the post-buckling stiffness to the pre-buckling stiffness can be calculated from Eq. (75) in a very straightforward manner.

$$\frac{S^*}{S} = 1 - \frac{\lambda^2 m_2}{8m_4 \sum b} \sum_0^b \int (f_{w1}^2 + 2\psi'' \cos(2\lambda x)) dy \tag{75}$$

where $\sum b$ is the width of the plate.

It is noted that in contrast to some other approximate analyses such as finite element method or conventional finite strip methods, the current exact analysis always leads to considerable reductions in computational time.

3. Theoretical development of the semi-analytical FSM

The theoretical development of the Semi-analytical Finite Strip Method (S-a FSM) for the analysis of the plates is presented in this section. The displacement fields of the S-a FSM are expressed as

$$u = -\varepsilon x + \sum_{n=1}^{ru} f_u^{(n)}(y) \sin\left(\frac{n\pi x}{L}\right) \tag{76}$$

$$v = v \varepsilon y + \sum_{n=0}^{rv} f_v^{(n)}(y) \cos\left(\frac{n\pi x}{L}\right) \tag{77}$$

$$w = \sum_{n=1}^{rw} f_w^{(n)}(y) \sin\left(\frac{n\pi x}{L}\right) \tag{78}$$

It is noted that ru , rv and rw represent the number of longitudinal terms assumed for the corresponding displacement functions. The $f_u^{(n)}$, $f_v^{(n)}$ and $f_w^{(n)}$ are transverse polynomial interpolation functions of various types and orders, involving undetermined displacement coefficients corresponding to the n th series' term along the length of the strip. In representing u and v variations across a strip, the linear Lagrange polynomial is used, and in representing w the cubic Hermitian polynomial is utilized as in most previous finite strip studies in the context of CPT, Ovesy and Ghannadpour and Morada 2005 and Ovesy and Ghannadpour 2006.

$$\begin{aligned} f_u(y) &= N_i u_i + N_j u_j \\ f_v(y) &= N_i v_i + N_j v_j \\ f_w(y) &= N_1^w w_i + N_2^w \theta_i + N_3^w w_j + N_4^w \theta_j \end{aligned} \tag{79}$$

where u_i, u_j, v_i and v_j are the undetermined in-plane nodal displacement parameters and w_i, w_j, θ_i and θ_j are the undetermined out-of-plane nodal displacement parameters along edges of the strip and

$$\begin{aligned}
N_1 &= 1 - \eta, & N_2 &= \eta \\
N_1^w &= 1 - 3\eta^2 + 2\eta^3, & N_2^w &= b(\eta - 2\eta^2 + \eta^3) \\
N_3^w &= 3\eta^2 - 2\eta^3, & N_4^w &= b(\eta^3 - \eta^2)
\end{aligned} \tag{80}$$

With the establishment of the finite strip displacement fields according to the equations that mentioned above, the strain energy of the strip U_s which is equal to its total potential energy V_s using Eqs. (2), (3), (6), (7), (8) and (9) can ultimately be expressed in the form

$$U_s = \frac{1}{2} \underline{\mathbf{d}}^T (\underline{\mathbf{k}}^{(0)} - \varepsilon \underline{\mathbf{k}}^*) \underline{\mathbf{d}} + \frac{1}{6} \underline{\mathbf{d}}^T \underline{\mathbf{k}}^{(1)} \underline{\mathbf{d}} + \frac{1}{12} \underline{\mathbf{d}}^T \underline{\mathbf{k}}^{(2)} \underline{\mathbf{d}} \tag{81}$$

Here $\underline{\mathbf{k}}^{(0)}$, $\underline{\mathbf{k}}^*$, $\underline{\mathbf{k}}^{(1)}$ and $\underline{\mathbf{k}}^{(2)}$ are symmetric square stiffness matrices. The coefficients of $\underline{\mathbf{k}}^{(0)}$ and $\underline{\mathbf{k}}^*$ are constant whilst those of $\underline{\mathbf{k}}^{(1)}$ and $\underline{\mathbf{k}}^{(2)}$ are linear and quadratic functions of the displacements, respectively. The column matrix $\underline{\mathbf{d}}$ contains the strip degrees of freedom. In evaluating U_s all integrations in the x and y directions are determined analytically.

For the whole plate, comprising an assembly of finite strips, the total potential energy is simply the summation of the potential energies of the individual finite strips. Correspondingly, whole plate matrices which are equivalent of those appearing in Eq. (81) for the individual finite strip are generated by appropriate summations in the standard fashion. Thus, the potential energy for whole plate can be expressed as

$$U_s = \frac{1}{2} \underline{\mathbf{D}}^T (\underline{\mathbf{K}}^{(0)} - \varepsilon \underline{\mathbf{K}}^*) \underline{\mathbf{D}} + \frac{1}{6} \underline{\mathbf{D}}^T \underline{\mathbf{K}}^{(1)} \underline{\mathbf{D}} + \frac{1}{12} \underline{\mathbf{D}}^T \underline{\mathbf{K}}^{(2)} \underline{\mathbf{D}} \tag{82}$$

The pertinent plate equilibrium equations are obtained by applying the principle of minimum potential energy. That is to say the partial differentiation of the plate potential energy with respect to each degree of freedom in turn gives a set of non-linear equilibrium equations

$$\left(\underline{\mathbf{K}}^{(0)} - \varepsilon \underline{\mathbf{K}}^* + \frac{1}{2} \underline{\mathbf{K}}^{(1)} + \frac{1}{2} \underline{\mathbf{K}}^{(2)} \right) \underline{\mathbf{D}} = 0 \quad \text{or} \quad \underline{\mathbf{K}} \underline{\mathbf{D}} = 0 \tag{83}$$

where $\underline{\mathbf{K}}$ is the global stiffness matrix, and $\underline{\mathbf{D}}$ is a vector, which includes the degrees of freedom for the whole structure. This set of equations needs to be modified by applying the appropriate zero-displacement boundary conditions at the longitudinal exterior edges of the plate (i.e., at the unloaded edges of the plate). After the application of any appropriate zero-displacement boundary conditions, the equations must be solved. In the present study the Newton-Raphson (N-R) iterative procedure is selected for solving the equations. Once the global equilibrium equations are solved and the nodal degrees of freedom are found for a particular prescribed end shortening, it is possible to calculate the displacements u , v and w at any point in any finite strip using Eqs. (76)-(78), and to determine force and moment quantities through use of Eq. (4).

The solution for the initial instability can be obtained by ignoring the nonlinear matrices $\underline{\mathbf{K}}^{(1)}$ and $\underline{\mathbf{K}}^{(2)}$ from Eq. (83)

$$(\underline{\mathbf{K}}^{(0)} - \varepsilon \underline{\mathbf{K}}^*) \underline{\mathbf{D}} = 0 \tag{84}$$

The eigenvalue problem of the above equation can be solved by using inverse iteration procedure that described in section Recursive Newton method (i.e., Eqs. (45) and (46)) to find the critical end-shortening strain ε_C .

4. Results and discussions

This section presents a number of numerical examples showing the excellent performance of the proposed algorithm, which was implemented in a Compaq Visual FORTRAN 6.5 computer program. It is noted that the program is run on a standard Pentium IV 3.0 GHz PC. The results of the developed F-a FSM analysis are compared with some other results which either have been taken directly from the literature or obtained from a S-a FSM analysis carried out by the authors.

In order to investigate the verification of the proposed method, the plate is divided into two, four, 10 and 50 strips of equal width giving four cases for consideration. The investigation of the results has revealed that the critical buckling load, the relative stiffness values and the post-buckling results are identical among the four cases as expected. Thus, a plate can be accurately modeled by applying only one strip to it. It is worth mentioning that the three error tolerances *Tol1*, *Tol2* and *Tol3* are taken to be 10^{-14} .

In the S-a FSM, in order to reflect the symmetry of the problem in the longitudinal direction, the appropriate series' terms are chosen and used. That is to say, for *u* the first three even terms ($n = 2, 4, 6$), for *v* the first four even terms ($n = 0, 2, 4, 6$) and for *w* the first two odd terms ($n = 1, 3$) were used. It is noted that for all the plates under consideration, the width to thickness ratio *b/t* and the Poisson's ratio ν are 120 and 0.3 respectively, and the plate is assumed to buckle into a single half-wave longitudinally.

4.1 Buckling results

In presenting the results in this section, two important parameters are now introduced

$$\phi = \frac{L}{b}$$

$$K = \frac{\sigma t b^2}{\pi^2 D} = \zeta \left(\frac{1}{\phi} \right)^2 \tag{85}$$

where *K* is the non-dimensional buckling coefficient and ϕ is the aspect ratio of the plate.

In order to investigate the convergence characteristics of recursive Newton method, the buckling of a plate with clamped-free boundary conditions (i.e., C-F) and aspect ratio of $\phi = 2$ is studied. The convergence results for the buckling coefficient are given in Table 1. It is noted that the buckling coefficient interval (K_U, K_L), in which $N_r = 1$ and $N_{r,0} = 0$, is (1.1,2). It can be seen in Table 1 that the algorithm has worked very satisfactorily by converging to $K^{(4)}$ with the accuracy of 14 decimal digits only after four iterations.

Table 1 Convergence procedure in recursive Newton method for plate C-F

κ	μ	K_μ	$K^{(\kappa)}$	μ -check
0			1.55000000000000	
1	0.21314086226485	1.33685913773515	1.33685913773515	Accept
2	0.00088210053354	1.33597703720161	1.33597703720161	Accept
3	0.00000001483335	1.33597702236826	1.33597702236826	Accept
4	0.00000000000000	1.33597702236826	1.33597702236826	Accept

Table 2 Comparison of the buckling coefficients (K) obtained by F-a FSM and S-a FSM

Case	Edges BCs	ϕ (L/b)	(K_L, K_U)	Buckling coefficient (K)		
				Run time(s), No. of strips, [No. of iterations in F-a FSM]		
				F-a FSM		S-a FSM
			Newton	Bisection		
1	S-F	1	(1.1,2)	1.40159812598470 0.02,1,[4]	1.40159812598470 0.08,1,[53]	1.40159812589585 2.2,90
2	S-S	1	(2,5)	4.00000000000000 0.02,1,[5]	4.00000000000000 0.07,1,[50]	4.0000000021518 3.61,100
3	C-F	1	(1.1,2)	1.65250589714372 0.02,1,[4]	1.65250589714372 0.07,1,[49]	1.65250589734019 3.1,100
4	C-F	2	(1.1,2)	1.33597702236826 0.02,1,[4]	1.33597702236826 0.07,1,[49]	1.33597702122061 4.17,100
5	C-S	1	(3,6)	5.74020783895471 0.02,1,[7]	5.74020783895471 0.07,1,[50]	5.74020781067525 14.66,170
6	C-C	0.5	(5,9)	7.69128364530829 0.02,2,[5]	7.69128364530829 0.1,2,[51]	7.69128365234950 13.77,180
7	C-C	2/3	(5,9)	6.97160208744291 0.02,2,[4]	6.97160208744291 0.1,2,[51]	6.97160215017088 15.46,180

S, C and F denote simply supported, clamped and free respectively.

Table 2 represents the numerical values of the buckling coefficient K obtained by the developed method (F-a FSM), both by the application of bisection and recursive Newton solvers, as well as the results obtained by the S-a FSM for different plates. The computer run time is represented in the table, and the number of finite strips that is served in the analysis is also inserted in the table. It is worth mentioning that for S-a FSM approach, the number of finite strips represented in the table are those obtained after the pertinent convergence studies with regard to the number of strips have been carried out. In the third column of Table 2, the buckling coefficient interval (K_U, K_L) , in which $N_r = 1$ and $N_{r0} = 0$, that is computed by the W-W algorithm is represented.

The table shows that the results of the buckling coefficient K that are obtained by both bisection and recursive Newton solvers are exactly the same. However, the number of iterations required by the recursive Newton solver to converge into the exact solution is less than those required by the bisection solver. For example, in the case four in Table 2, which is the same plate as that investigated earlier in Table 1, bisection method requires at least 49 bisections in order to converge to an approximate buckling coefficient with accuracy comparable to that of $K^{(4)}$ in Table 1.

The table also shows that the results of the F-a FSM agree very well with those obtained by S-a FSM. It is noted that for a given degree of accuracy in the results, the F-a FSM analysis requires much less computational effort, as a consequence of implementing less degrees of freedom, compared to the S-a FSM.

For completeness, the buckling mode shape of a representative plate, i.e., the case four in Table 2, is shown in Fig. 2. A very good agreement can be seen among the mode shapes obtained by different methods.

It is worth pointing out that in the remainder of the present paper, the F-a FSM is to be carried out using recursive Newton method as distinct from the bisection method.

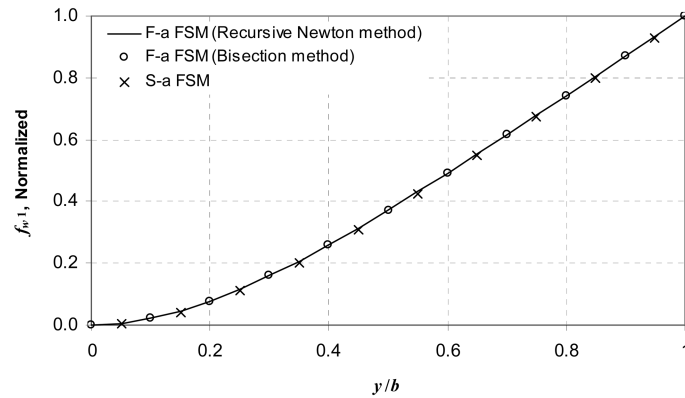


Fig. 2 Out-of-plane buckling deflection mode in transverse direction for plate C-F

4.2 Relative stiffness and post-buckling behaviour

Table 3 represents the numerical values of the relative stiffness (i.e., the S^*/S at the instant of buckling) for different plates. The presented values consist of those derived from the developed F-a FSM analysis and those from Ref. Rhodes and Harvey 1974. The values of the relative stiffness provided by Rhodes and Harvey 1974 have been calculated by implementing a semi-energy technique. These values are accurate because, in their calculation process, the postulated deflected form after buckling has been taken as the buckling solution. However, in their buckling analysis, in contrast to the current F-a FSM where the Von-Karman's equilibrium equation is solved exactly to obtain the buckling coefficients and corresponding mode shapes, the principle of Minimum Potential Energy is used to obtain the buckling coefficients and mode shapes. Thus, the values of relative stiffness acquired by the developed F-a FSM analysis are exact and the corresponding results of Rhodes and Harvey 1974 are somewhat approximate.

It is worth mentioning that in the other approximate methods such as Finite Element Method (FEM), S-a FSM, semi-energy FSM or Spline FSM, the calculation of the values of relative stiffness is very time consuming due to the incremental nature of the solution strategy in these methods.

Table 3 Comparison of the F-a method results (S^*/S) with the results of Rhodes

Case	Edges BCs		ϕ (L/b)	Relative Stiffness (S^*/S)	
	In-plane	Out-of-plane		F-a FSM	Rhodes
1	Unconstrained	S-S	1	0.40833586	0.408
2	Straight	S-S	1	0.50000000	---
3	Unconstrained	S-F	2	0.43699398	0.438
4	Unconstrained	C-S	1	0.49405703	0.494
5	Unconstrained	C-F	2	0.55666462	0.556
6	Unconstrained	C-C	2/3	0.48128190	0.481

For the in-plane conditions, Straight denotes that the unloaded edges are kept straight but allowed to move in-plane.

Figs. 3-7 show the variation of the relative stiffness, i.e., S^*/S at the instant of buckling, with the aspect ratio ϕ . In these figures, the two loaded edges of the plate are simply supported whilst the boundary conditions at the two unloaded edges are of a variety of combinations, namely simply-simply (S-S), clamped-clamped (C-C), clamped-simply (C-S), clamped-free (C-F) and simply-free (S-F) in Figs. 3-7, respectively. It is seen in all the figures that the relative stiffness is increased by the increase in the aspect ratio. Obviously, if the number of buckle half-waves were allowed to take values more than 1, i.e., the constant value assumed so far in the current study, the afore-mentioned behavior might change accordingly. This investigation is also carried out and the results are presented in Fig. 8. It is seen in Fig. 8 that by allowing the change in the number of buckle half-waves n to occur, the buckling coefficient variations demonstrate a clear garland type behavior. Moreover, it is interesting to note that for certain aspect ratios at which the switching in the number of buckle half-waves is experienced by the buckling coefficient variations, a sudden drop in the values of the relative stiffness, i.e., S^*/S at the instant of buckling, is demonstrated.

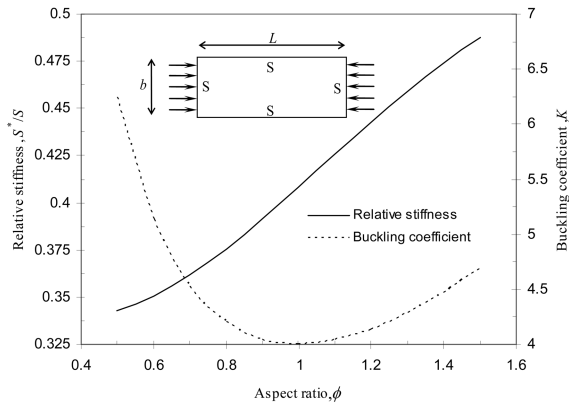


Fig. 3 Relative stiffness and buckling coefficient for plates having two longitudinal edges simply supported

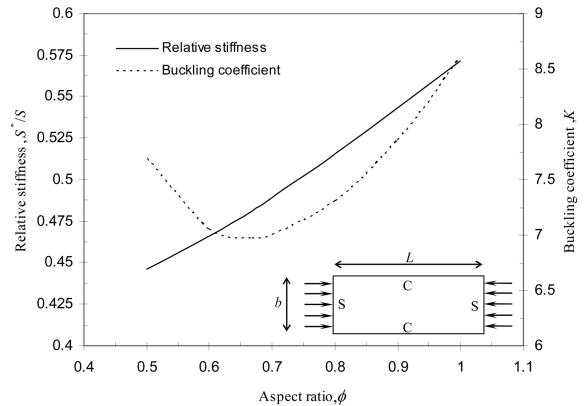


Fig. 4 Relative stiffness and buckling coefficient for plates having two longitudinal edges clamped

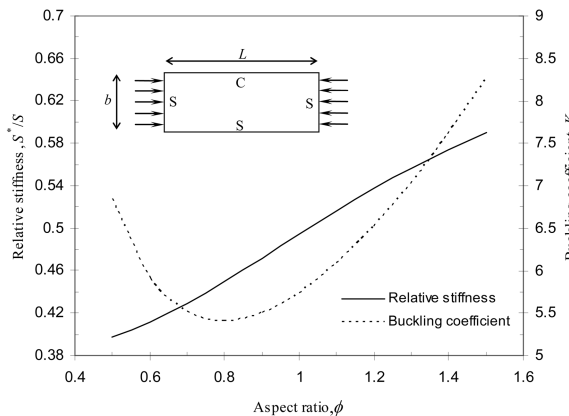


Fig. 5 Relative stiffness and buckling coefficient for plates having one longitudinal edge simply supported, one clamped

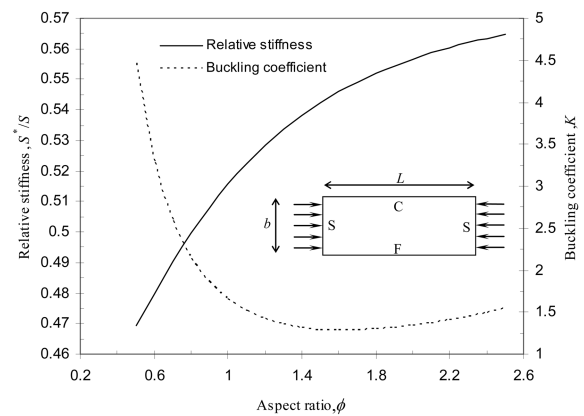


Fig. 6 Relative stiffness and buckling coefficient for plates having one longitudinal edge clamped, one free

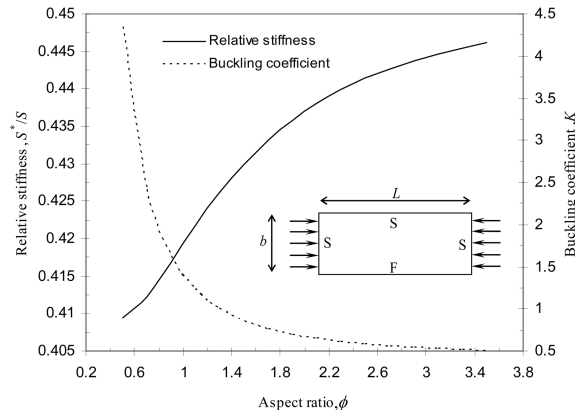


Fig. 7 Relative stiffness and buckling coefficient for plates having one longitudinal edge simply supported, one free

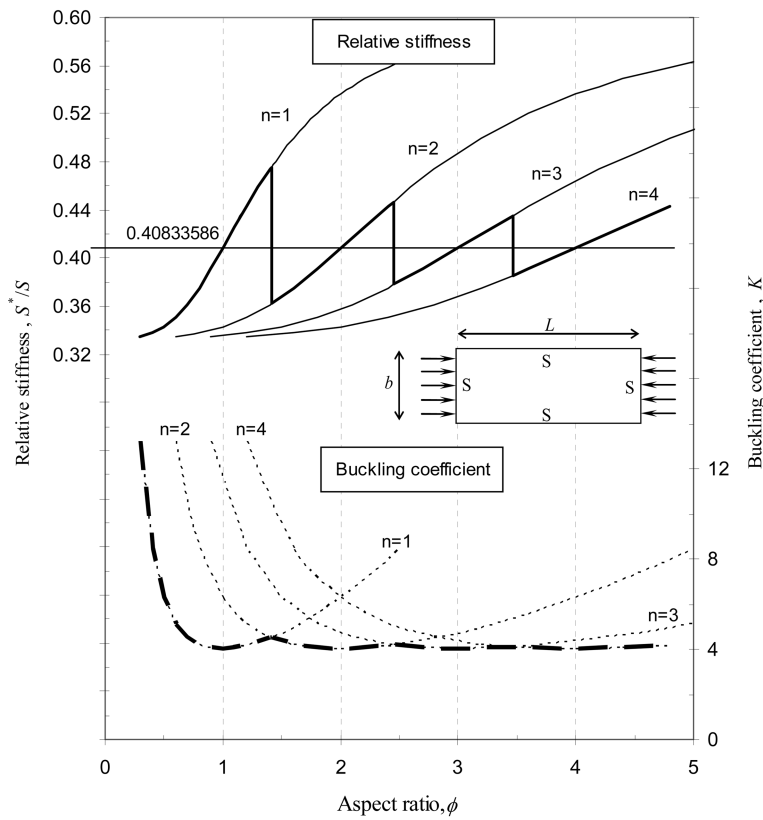


Fig. 8 The variation of relative stiffness and buckling coefficient for simply supported plates

The next step is to compare the F-a FSM results with those from S-a FSM inside the post-buckling range. The non-dimensional form of load-end shortening variation ($P/P_{Cr} - \varepsilon/\varepsilon_{Cr}$) and the non-dimensional form of load-peak deflection variation ($P/P_{Cr} - w_{2max}/t$) for the C-F plate with

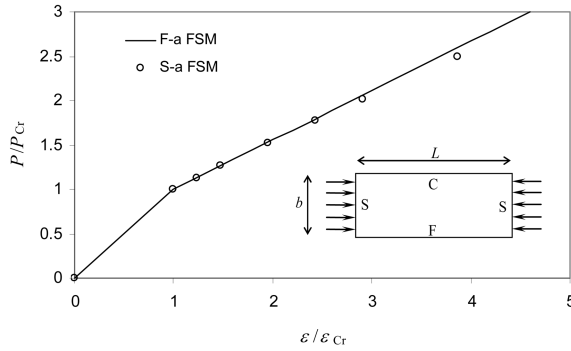


Fig. 9 Non-dimensional load-end shortening variation for C-F plate

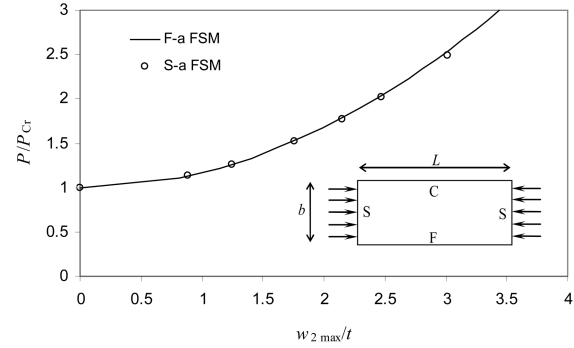


Fig. 10 Non-dimensional load-peak deflection variation for C-F plate

aspect ratio ϕ equal to 2, i.e., the case four in Table 2 or the case five in Table 3, are depicted in Figs. 9 & 10, respectively.

It is noted that in the pre-buckling range (i.e., for $\varepsilon/\varepsilon_{cr}$ and P/P_{cr} between 0 to 1) the out-of-plane deflection is zero, and thus as expected a clearly linear behaviour (see Fig. 9) is predicted by both F-a FSM and S-a FSM approaches.

It may be noted that in the post-buckling range, the peak deflection occurs at the crest of the buckle at the free edge of the plate. Having carried out a collapse investigation similar to that attempted in Ref. Ovesy, Loughlan and Ghannadpour 2005, it is revealed that the collapse of the C-F plate does not take place within the range of loading shown in these figures. Thus, the validation of the F-a FSM analysis will be discussed for the entire range of loading presented in the figures. The results obtained by S-a FSM are presented so that they can be compared with those obtained using the developed F-a FSM. Before making any comment on how the results compare with each other, a brief description on the assumption of constant stiffness in the post-buckling stage is given below.

As it can be seen in Eq. (74), the relationship between P and ε in the post-buckling region is a linear function, i.e., the post-buckling stiffness in the case of F-a FSM analysis is constant for the entire range of post-buckling. Obviously, this constant stiffness is equal to the slope of the tangent to the actual post-buckling curve at the buckling point. It is worth mentioning that the single term assumption within F-a FSM analysis corresponds to the fact that the shape of the plate in the post-buckling region is unchangeable in both longitudinal and transverse directions. Thus, the relationship between P and ε has become a linear function. However in the case of S-a FSM analysis, a clearly non-linear behaviour is expected to occur due to the fact that the longitudinal change has been allowed by the multi-term nature of the analysis, and the transverse change has been allowed by the finite strip nature of the analysis.

As far as the comparison between F-a FSM and S-a FSM results is concerned, Fig. 9 shows a good agreement between the load-end shortening variation results over the entire range of loading under consideration, and Fig. 10, in general, indicates a very good agreement over the range of loading shown in the figure.

It is emphasized that the convergence studies with regard to the number of strips have been investigated for the entire S-a FSM results presented in the figures. It is noted that 32 finite strips are proved to be sufficient to obtain converged results.

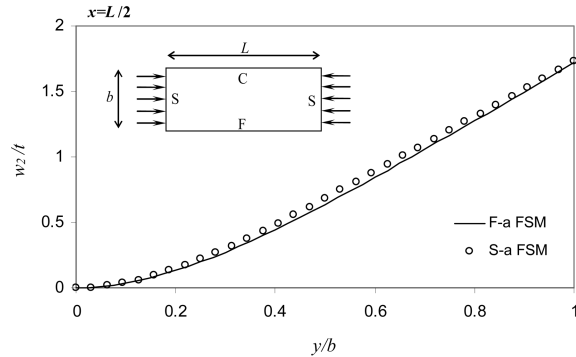


Fig. 11 The out-of-plane deflected shape across the C-F plate at the crest of the buckle at load $P = 1.5P_{Cr}$

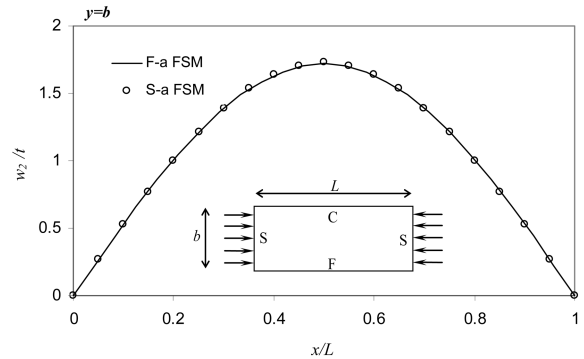


Fig. 12 The out-of-plane deflected shape along the length at the free edge of the C-F plate at load $P = 1.5P_{Cr}$

Figs. 11 to 13 show the comparison of a variety of different F-a FSM results with the corresponding S-a FSM results at a load of $P = 1.5P_{Cr}$. The out-of-plane deflected shape of the plate is shown in Figs. 11 and 12. Fig. 11 depicts the deflected shape across the plate at the crest of the buckle, and Fig. 12 shows the buckle form along the length at the free edge of the plate. Although at some of the locations a small difference between the results can be seen, the consistency between the results is very good in general.

Fig. 13 depicts the non-dimensional form of longitudinal mid-plane σ_x stress distributions across the plate at three different cross sections along the length, i.e., node, average (midway between node and crest) and crest of buckle. A very good agreement between F-a FSM and S-a FSM results can be seen at all of the cross sections of the plate. It is evident that, at all of the cross sections, the load is shed towards the clamped edge of the plate. This load shedding occurs due to the growth in the out-of-plane deflection across the plate in the post-buckling region. This deflection grows faster at the crest of buckling in the regions near to the free edge of the plate. Hence these regions become less capable of carrying compressional load and as a result tend to shed the load towards the clamped edge. This load shedding takes place to such an extent that the stresses become tensile at the free edge of the plate. It may be noted that the maximum edge stress occurs at the crest of buckling at the clamped edge of the plate.

Finally, it has become clear that regardless of the plate's aspect ratio and boundary conditions, both F-a FSM and S-a FSM approaches are capable of delivering excellent results for predicting the post-buckling behavior of the plates. As far as the comparison of the results is concerned, it is sometimes seen that the results are different from each other by a small amount. In general, however, the agreement between the results is very good. It may be noted that the reason for the small difference between the results may lie with the fact that the F-a FSM utilizes a single term to represent the out-of-plane deflection whilst in the case of the S-a FSM method the formulations are based on a multi-term approach. It is noted that for a given degree of accuracy in the results, the F-a FSM analysis requires less computational effort, as a consequence of implementing less degrees of freedom, compared to the S-a FSM.

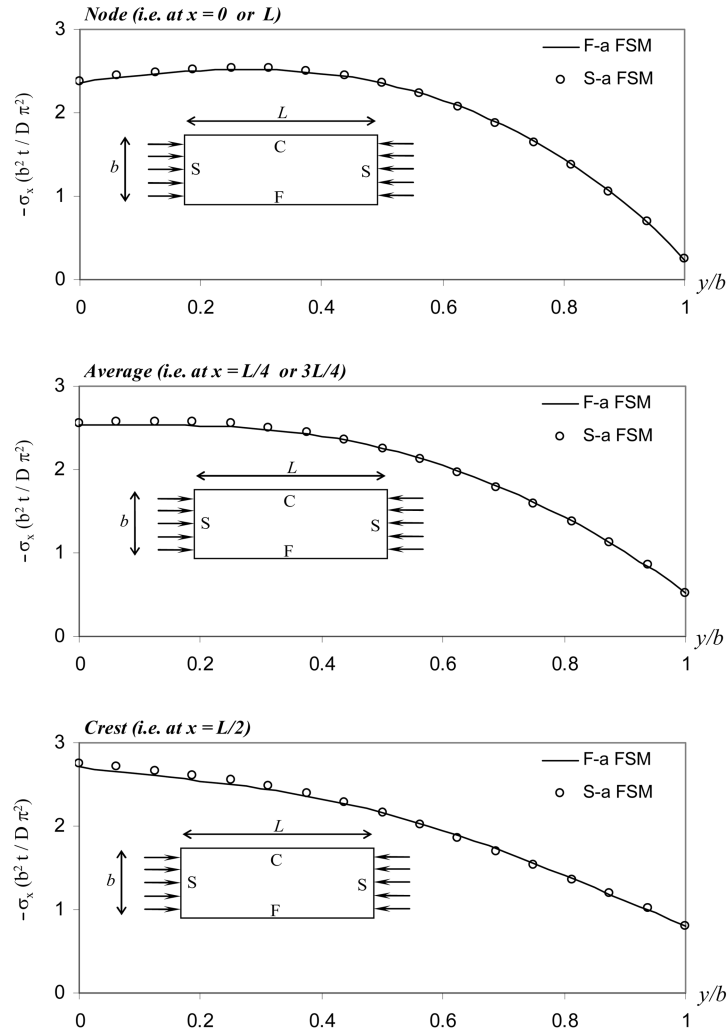


Fig. 13 Longitudinal mid-plane stress distributions across the C-F plate at load $P = 1.5P_{Cr}$.

5. Conclusions

Theoretical developments of an exact finite strip for the buckling and initial post-buckling analyses of isotropic flat plates have been presented. The so-called exact finite strip has been assumed to be simply supported out-of-plane at the loaded ends. The strip has been developed based on the concept that it is effectively a plate, and thus the Von-Karman's equilibrium equation has been solved exactly to obtain the general form of out-of-plane buckling deflection mode for the corresponding plate/strip. The investigation of thin flat plate buckling behavior is then extended to an initial post-buckling study with the assumption that the deflected form immediately after the buckling is the same as that obtained for the buckling. The Von-Karman's compatibility equation has been solved exactly to obtain the general form of in-plane displacement fields in the post-buckling region. The obtained in-plane and out-of-plane deflected functions are then substituted in

the total strain energy expressions and the theorem of minimum total potential energy is invoked. The developed method is subsequently applied to analyze the buckling and initial post-buckling behavior of some representative thin flat plates. The presented buckling results have indicated the capability of the developed F-a FSM analysis in terms of delivering exact results at buckling point. The values of relative post-buckling stiffness obtained by the developed F-a FSM analysis are also extremely accurate at the buckling point because the exact buckling mode shape and corresponding buckling coefficient are used in the post-buckling analysis.

Having compared the F-a FSM results with those from Semi-analytical FSM inside the post-buckling range, a small difference between the results is experienced. This has been due to the fact that the current F-a FSM analysis utilizes only a single term to represent the out-of-plane deflection in the post-buckling region. However, for a given degree of accuracy in the results, the F-a FSM analysis requires less computational effort, as a consequence of implementing less degrees of freedom, compared to the S-a FSM.

Finally, it is worth mentioning that the promising results obtained in the current paper have made the authors to extend the application of F-a FSM analysis to the post-local-buckling analysis of plate structures, i.e., short struts. Some interesting results have already been obtained which will be published once the investigation is complete.

References

- Bathe, K.J. (1996), *Finite Element Procedures*, Prentice-Hall, Englewood Cliffs, NJ.
- Cheung, Y.K. and Kong, J. (1995), "The application of a new finite strip to the free vibration of rectangular plates of varying complexity", *J. Sound Vib.*, **181**, 341-353.
- Chou, S.M. and Rhodes, J. (1997), "Review and compilation of experimental results on thin-walled structures", *Comput. Struct.*, **65**, 1, 47-67.
- Dawe, D.J. and Craig, T.J. (1988), "Buckling and vibration of shear deformable prismatic plate structures by a complex finite strip method", *Int. J. Mech. Sci.*, **30**, 77-79.
- Dawe, D.J. and Wang, S. (1996), "Postbuckling analysis of thin rectangular laminated plates by spline FSM", *Published in the Conference Proceedings of "Bicentenary Conference on Thin-Walled Structures"*, University of Strathclyde, UK, December.
- Dawe, D.J. (2002), "Use of the finite strip method in predicting the behaviour of composite laminated structures", *Comp. Struct.*, **57**, 11-36.
- Graves Smith, T.R. and Sridharan, S. (1978), "A finite strip method for the post-locally-buckled analysis of plate structures", *Int. J. Mech. Sci.*, **20**, 833-842.
- Hancock, G.J. (1981), "Nonlinear analysis of thin sections in compression", *J. Struct. Div.*, ASCE, **107**(ST3), 455-471.
- Khong, P.W. and Rhodes, J. (1988), "Linear and non linear analysis on the micro using finite strip", in "*SAM 88 Stress Analysis and the Micro*", (Edited by A. L. Yettram), 25-35, IOP, London.
- Kong, J. and Cheung, Y.K. (1995), "A generalized spline finite strip for the analysis of plates", *Thin Wall. Struct.*, **22**, 181-202.
- Kwon, Y.B. and Hancock, G.J. (1992), "Post-buckling analysis of thin-walled channel sections undergoing local and distortional buckling", *Research Report, No. R650, School of Civil and Mining Engineering*, the University of Sydney, Australia.
- Lau, S.C.W. and Hancock, G.J. (1986), "Buckling of thin flat-walled structures by a spline finite strip method", *Thin Wall. Struct.*, **4**, 269-294.
- Marguerre, K. (1937), "The apparent width of plates in compression", *NACA Technical Memorandum No. 833, National Advisory Committee for Aeronautics*, Washington, D.C.
- Ovesy, H.R., Loughlan, J. and Assaee, H. (2004), "The compressive post-local buckling behaviour of thin plates

- using a semi-energy finite strip approach”, *Thin Wall. Struct.*, **24**, 449-474.
- Ovesy, H.R., Loughlan, J and Ghannadpour, S.A.M. (2005), “Geometric non-linear analysis of thin flat plates under end shortening, using different versions of the finite strip method”, *Int. J. Mech. Sci.*, **47**, 1923-1948.
- Ovesy, H.R., Ghannadpour, S.A.M. and Morada, G. (2005), “Geometric non-linear analysis of composite laminated plates with initial imperfection under end shortening, using two versions of finite strip method”, *Comp. Struct.*, **71**, 307-314.
- Ovesy, H.R., Loughlan, J. and Ghannadpour, S.A.M. (2006), “Geometric non-linear analysis of channel sections under end shortening, using different versions of the finite strip method”, *Comput. Struct.*, **84**, 855-872.
- Ovesy, H.R., Loughlan, J., Ghannadpour, S.A.M. and Morada, G (2006), “Geometric non-linear analysis of box sections under end shortening, using three different versions of the finite strip method”, *Thin Wall. Struct.*, **44**, 623-637.
- Ovesy, H.R. and Ghannadpour, S.A.M. (2006), “Geometric nonlinear analysis of imperfect composite laminated plates, under end shortening and pressure loading, using finite strip method”, *Comp. Struct.*, **75**, 100-105.
- Rhodes, J. and Harvey, J.M. (1977), “Examination of plate post-buckling behaviour”, *J. Eng. Mech.*, ASCE, **103**, No. EM3, 461-478.
- Rhodes, J. (1996), “Research into thin walled structures at the university of strathclyde - a brief history”, *Published in the Conference Proceedings of “Bicentenary Conference on Thin-Walled Structures”*, University of Strathclyde, UK, December.
- Sridharan, S. and Graves Smith, T.R. (1981), “Post-buckling analyses with finite strips”, *J. Eng. Mech.*, ASCE, **107**, 869-888.
- Wang, S. and Dawe, D.J. (1999), “Buckling of composite shell structures using the spline finite strip method”, *Composites: Part B*, **30**, 351-364.
- Wilkinson, J.H. (1965), *The Algebraic Eigenvalue Problem*, Clarendon, Oxford.
- Williams, F.W. and Wittrick, W.H. (1970), “An automatic computational procedure for calculating natural frequencies of skeletal structures”, *Int. J. Mech. Sci.*, **12**, 781-791.
- Wittrick, W.H. and Williams, F.W. (1971), “A general algorithm for computing natural frequencies of elastic structures”, *Q. J. Mech. Appl. Math.*, **24**, 263-284.
- Wittrick, W.H. and Williams, F.W. (1973), “An algorithm for computing critical buckling loads of elastic structures”, *J. Struct. Mech.*, **1**, 497-518.
- Wittrick, W.H. and Williams, F.W. (1974), “Buckling and vibration of anisotropic or isotropic plate assemblies under combined loading”, *Int. J. Mech. Sci.*, **16**, 209-239.
- Yuan, S., Ye, K., Williams, F.W. and Kennedy, D. (2003), “Recursive second order convergence method for natural frequencies and modes when using dynamic stiffness matrices”, *Int. J. Numer. Meth. Eng.*, **56**, 1795-1814.
- Zou, G.P. and Lam, S.S.E. (2002), “Buckling analysis of composite laminates under end shortening by higher-order shear deformable finite strips”, *Int. J. Numer. Meth. Eng.*, **55**, 1239-1254.